Correlation Between Elastic Properties and Phase Transformation of $Zr_{50}Pd_{50-x}Ru_x$ High-Temperature Shape Memory Alloys Designed by DFT

YU-NIEN SHEN, D. NKOMO, S. MATSUNAGA, M.J. PHASHA, and Y. YAMABE-MITARAI

The effect of Ru addition on the martensitic transformation and mechanical properties of $Zr_{50}Pd_{50-x}Ru_x$ SMAs shape memory alloys has been studied. Strain–temperature experiments, differential scanning calorimeter, and scanning electron microscope analyses were performed to validate the theoretical predictions by DFT calculation regarding the influence of the C' parameter on martensitic stability. Despite the absence of an observed shape memory effect under the tested conditions, the findings suggest that ZrPdRu alloys hold promise for high-temperature applications.

https://doi.org/10.1007/s11661-024-07502-9

THE study of high-temperature shape memory alloys (HT-SMAs) has increasingly captured the interest of the materials science community, primarily due to the growing demand for materials that can function effectively under extreme conditions. Conventional shape memory alloys, such as TiNi, frequently face limitations in certain applications due to their transformation temperature restrictions, which are typically below 100 °C.[1] This limitation has led to research into alternative materials, such as TiPd alloys from the HT-SMA family, which demonstrate martensitic transformation temperatures (MTTs) exceeding 500 °C. However, these alloys face challenges in achieving complete strain recovery because of plastic deformation at high temperature.[2]

In this context, ZrPd alloys emerge as a significant alternative. As binary shape memory alloys, the ZrPd series undergoes a martensitic transformation with an austenite transformation finish temperature (A_f) exceeding 600 °C. This property uniquely positions them at the forefront of HT-SMA research. Differing structurally from TiPd HT-SMAs, these alloys transition thermo-elastically from a cubic B2-type austenite phase to orthorhombic B33-type martensitic phases, offering a unique path in the exploration of high-temperature shape memory materials.[3,4]

Recent progress in the Zr–Pd phase diagram has revealed the existence of new intermediate phases, suggesting behavior to be more complex than previously understood.[5] Additionally, the exploration of ternary alloys such as ZrCoPd has emphasized the important role of Pd in enhancing ductility through transformation-induced plasticity, crucial for SMA functionality.[6] The thermoelastic martensitic transformation in these alloys, especially the transition from B2 to B33 structure, involves a mix of six distinct variants.[7,8] These variants are crucial for the self-accommodation mechanism, visualizing the potential to achieve desired shape memory effects and superelastic properties. However, despite these theoretical and microstructural insights, there are still uncertainties about the full potential of ZrPd alloys with B33 martensite as high-temperature SMAs, due to the limited investigation of their mechanical properties and the actual demonstration of the shape memory effect.

Notably, some research in ZrPd alloys have shown that these alloys undergo a martensitic transformation from a cubic B2-type parent phase to an orthorhombic and monoclinic martensitic phase at elevated temperatures.[3] Understanding these transformation phenomena and phase balances is crucial for developing new HT-SMAs. Experimental studies have reconstructed the ZrPd binary phase diagram, revealing critical transformations like eutectoid and peritectoid reactions at

YU-NIEN SHEN, S. MATSUNAGA, and Y. YAMABE-MITARAI are with the Department of Advanced Materials Science, The University of Tokyo, 5-1-5 Kashiwanoha, Kashiwa-shi, Chiba 277-8561, Japan. Contact e-mail: mitarai.yoko@edu.k.u-tokyo.ac.jp D. NKOMO is with the Advanced Materials Division, MINTEK, 200 Malibongwe Drive, Randburg 2194, South Africa and also with the Department of Materials Science and Metallurgical Engineering, University of Pretoria, Hatfield, Pretoria 0028, South Africa. M.J. PHASHA is with the Advanced Materials Division, MINTEK.
Manuscript submitted March 21, 2024; accepted June 24, 2024.
Article published online July 13, 2024

specific temperatures, further complicating the understanding of these alloy systems.[9]

Employing density functional theory (DFT)-based first-principles calculations, Nkomo *et al.*, investigated the stability of the B2 structure of ZrPd.[10] They tried to find the optimal convergence criteria to predict reliable elastic properties that underpin the SMA behavior using DFT calculations.[11] The reliability of these predictions heavily depends on the carefully selecting energy cutoffs and k-points, both of which are crucial for ensuring accuracy of the results.[12,13]

In this study, we aim to experimentally validate the theoretical predictions made by DFT calculations regarding the potential for HT-SMAs, focusing on the mechanical properties of the ZrPd binary alloy and alloys with Ru, which can stabilize the B2 structure. Our research specifically targets the C' parameter (tetragonal shear modulus), which is considered to indicate the mechanical stability of the B2 phase.[11] By doing so, we intend to provide concrete evidence that supports or refines the DFT predictions made by Nkomo. This work is essential in narrowing the gap between computational forecasts and experimental realities, particularly in the context of ZrPd alloys' martensitic transformations and shape memory behaviors.

In the experiment, five $Zr_{50}Pd_{50-x}Ru_x$ alloys, with x values of 0, 6.25, 12.5, 18.75, and 20 (atomic pct), were melted using a vacuum arc melting under an argon atmosphere. These alloys were designated as Ru0, Ru6.25, Ru12.5, Ru18.75, and Ru20, corresponding to their respective Ru content. To minimize oxygen contamination, a pure titanium getter was remelted twice prior to each alloy melting process. Each ingot underwent multiple melting and flipping processes at least six times to ensure desired alloy composition was achieved. Subsequently, these ingots were homogenized in evacuated quartz tubes, filled with an argon atmosphere, at 1200 °C for 3 hours and then quenched in water. The thermal behavior of the alloys was analyzed using a differential scanning calorimeter (DSC, Q10, TA instruments) (DSC, 3200S, NETZSCH, Japan), which measured heat flows during both cooling and heating at a rate of 10 °C/min. The microstructural characteristics were examined using a field-emission scanning electron microscope (SEM, JSM-7600F, JEOL, Japan) equipped with an energy-dispersive X-ray (EDS) detector. To obtain diffraction spectra, an X-ray diffractometer (XRD, RINT, Rigaku, Japan) with a heating stage was employed. The shape memory effects of these SMAs were assessed through strain–temperature testing (ST test, AG-X, SHIMADZU, Japan). Specimens for this test, measuring 3 × 3 × 5.5 mm, were initially subjected to a compressive stress of 50 MPa and then underwent thermal cycling at a heating/cooling rate of 40 °C/min. With each subsequent cycle, the applied stress was increased by 50 MPa. After each cycle, both the recoverable and irrecoverable strains were calculated from the strain–temperature curves. Temperature control during the tests was maintained using an induction heating, while a CCD camera recorded the strain experienced by the specimens.

The XRD results for alloys Ru0 to Ru20, both at room temperature and high temperature, are presented in Figure 1. Ru0 in Figure 1(a) shows the presence of a monoclinic phase peak at room temperature for Ru0, consistent with the previous research findings. Conversely, Figure 1(b) displays peaks corresponding to the B33 martensite phase at room temperature, indicating that the transformation temperatures for Ru6.25 are above room temperature. Also, the presence of B2 peaks during measurement at 700 °C in Ru6.25 [Figure 1(b)] indicates their high-temperature phase as B2 austenite phase. In contrast, Ru12.5, as shown in Figure 1(c), displays mixed peaks of both B2 austenite and B33 martensite phases at room temperature. This suggests that the martensite finish temperature (M_f) for Ru12.5 is below room temperature, further indicating it is lower than that of Ru0 and Ru6.25. Conversely, the presence of pure B2 peaks at 600 °C in Ru12.5 indicates that the high-temperature phase is the B2 austenite phase. In Figures 1(d) and (e), Ru18.75 and Ru20 exclusively show B2 austenite phase peaks, suggesting that their martensite start temperatures (M_s) are beneath room temperature. Furthermore, to compare the volume of B2 and B33 phase, we calculate the volume of the unit lattice of two structures from XRD data divided by the number of atoms in a unit lattice as a ratio of volume/atom. The volume/atom ratio illustrated in Figure 1(f) reveals a significant decrease in B2 volume with the increase in Ru content, while B33 volume remains relatively constant. This observation suggests that incorporating Ru into ZrPd alters the volume change associated with the transformation, transitioning from contraction to expansion.

SEM images of all the alloys are depicted in Figure 2. In Figures 2(a) and (b), the homogenization process of Ru0 and Ru6.25 was fully completed. Consistent with the XRD patterns, Ru6.25 displays a uniform twin structure, whereas Ru12.5 exhibits a mixture of twin structure and austenite phases, including a noticeable dendritic structure as presented in Figure 2(c). Ru18.75 and Ru20 exhibit a more pronounced dendritic structure with multiple austenite phases [Figures 2(d) and (e)]. These results reveal that the homogenization process in some alloys was incomplete. The addition of Ru appears to raise the melting point of the alloys, thereby increasing the difficulty of achieving complete homogenization. Despite our efforts to replicate the heat treatment temperatures reported in other studies[13] and increase the homogenization temperature to 1500 °C, all alloys melted and reacted during heat treatment, casting doubt on the reliability of the heat treatment parameters reported in other publications.

The EDS results are summarized in Table I. In Ru12.5 and Ru18.75, as shown in Figures 2(c) and (d), respectively, the matrix is divided into two regions: one enriched in Pd and the other in Ru. In Ru20, as shown in Figure 2(e), a region with an even higher concentration of Ru was observed. Notably, the martensite twin structure is only observed in the Pd-rich regions, indicating that the presence of Ru suppresses martensitic transformation. This suppression leads to a reduction in

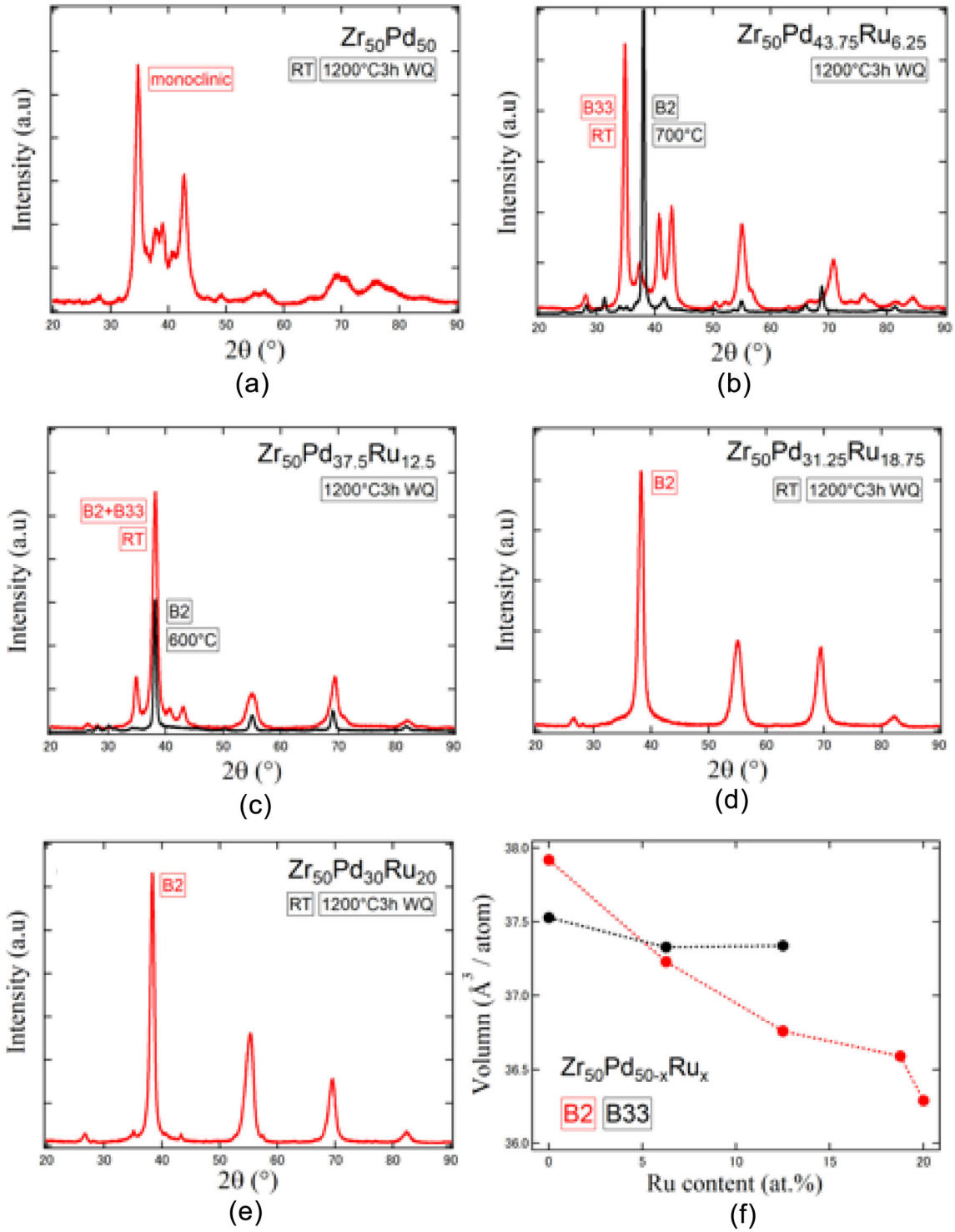

Fig. 1—X-ray diffraction (XRD) patterns observed at room temperature and elevated temperatures for samples: (*a*) Ru0, (*b*) Ru6.25, (*c*) Ru12.5, (*d*) Ru18.75, and (*e*) Ru20. (*f*) Presents the volume/atom ratio (lattice volume/*Z*) for B2 and B33 structures, calculated from the XRD data.

the regions capable of undergoing martensitic transformation at room temperature.

The DSC results for alloys Ru0 to Ru20 are shown in Figure 3. In Figures 3(a) and (b), both Ru0 and Ru6.25 display distinct transformation peaks during heating and cooling cycles. Ru0 exhibits an exceptionally high transformation temperature, with an A_f around 650 °C. Moreover, the transformation peak of Ru0 is notably sharp, indicating that transformation of all the specimen occurs at the almost same temperature, suggesting a high degree of homogeneity in the alloy. In contrast, Ru6.25 has a relatively lower transformation temperature, with an A_f around 600 °C as shown in Figure 3(b). However, its transformation peak is considerably

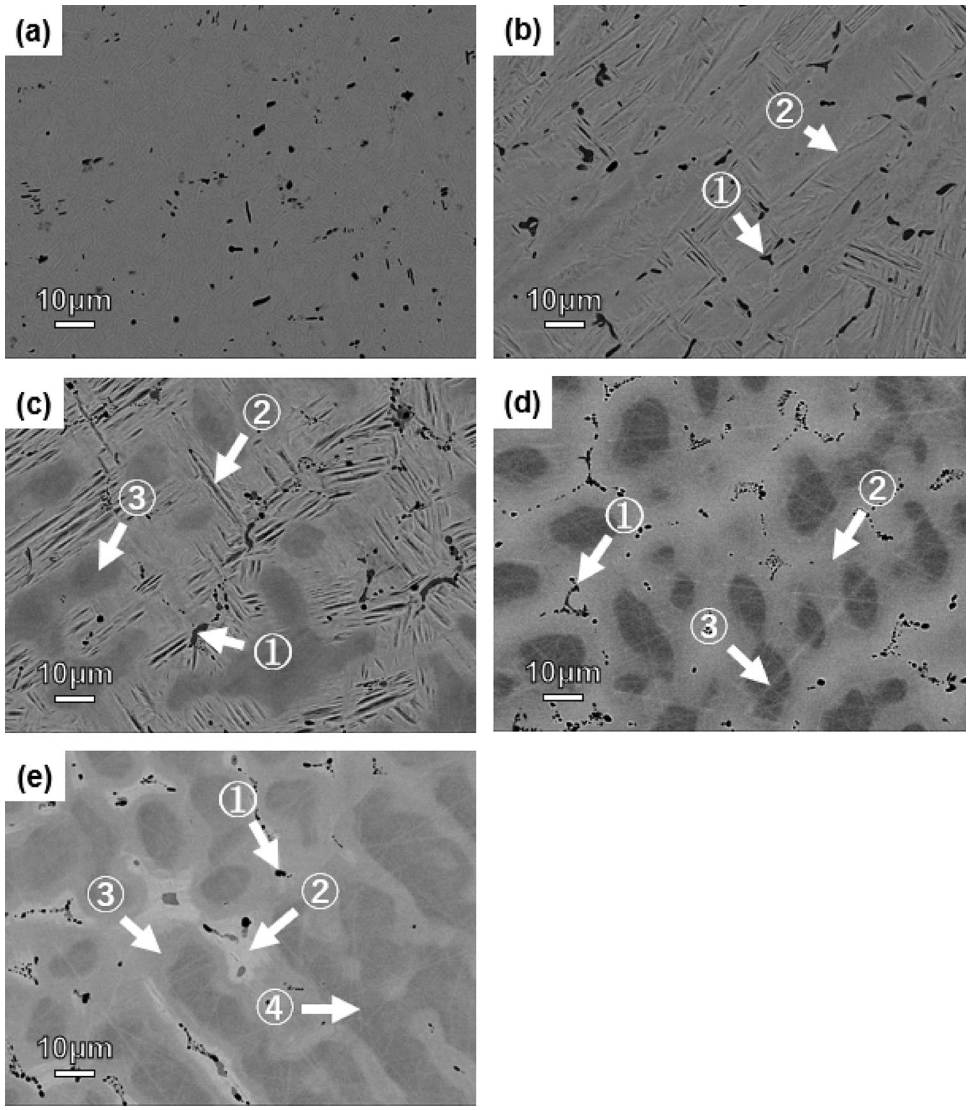

Fig. 2—Backscattered electron images of (*a*) Ru0, (*b*) Ru6.25, (*c*) Ru12.5, (*d*) Ru18.75, (*e*) Ru20 alloys after homogenized at 1200 °C for 3 hours.

broader than that of Ru0. The transformation temperature range ($A_f - A_s$) of Ru6.25 is about 200 °C, which is significantly wider than the 25 °C range observed in Ru0. This broadening of the transformation temperature range indicates that transformation in different regions occurred at different temperature levels. Different areas of slightly varying composition in atomic scale can be attributed to the addition of extra elements to the alloy, leading to this broadening effect. With further addition of Ru, as in Ru12.5, Figure 3(c), an even wider transformation range is observed. Interestingly, despite the presence of martensite at room temperature as seen under SEM, there are no clear transformation peaks in the DSC results of Ru12.5. Curves that look like peaks are present, but they are too indistinct to determine the transformation temperature accurately. Conversely, as shown in Figure 3(d) and (e), the results for Ru18.75 and Ru20 are more straightforward. No transformation peaks are observed in these alloys within the tested temperature range of − 100 °C to 700 °C. It is noteworthy that our results for the transformation temperatures differ significantly from those reported by Waterstrat *et al.*,[13] due to differences in our experimental approaches. This discrepancy highlights the need for further research to establish the correct homogenization method for ZrPdRu alloys. Nevertheless, our results align with the predictions from Nkomo's research.[10] Nkomo elucidated that introducing Ru into ZrPd alloys in place of Pd leads to an increase in the elastic property C', as shown in Figure 3(f), which in turn stabilizes the B2 structure and lowers the martensitic transformation temperature. Our observations support this theory; although the homogenization for some alloys was incomplete, focusing on the regions marked in Table I that exhibit martensite twins allows us to confirm that the transformation temperature significantly decreases as the Ru content increases. This trend distinctly demonstrates that the C' value has a

Table I. Phase Composition of Ru6.25, Ru12.5, Ru18.75, and Ru20

	Zr (At. Pct)	Pd (At. Pct)	Ru (At. Pct)	Martensite Twin
Ru6.25 ①	64.5	34.1	1.4	X
Ru6.25 ②	50.1	44.1	5.8	○
Ru12.5 ①	65.6	32.2	2.2	X
Ru12.5 ②	50.5	38.7	10.8	○
Ru12.5 ③	51.0	32.6	16.4	X
Ru18.75 ①	62.5	27.7	9.8	X
Ru18.75 ②	50.6	34.7	14.7	X
Ru18.75 ③	51.1	20.0	28.9	X
Ru20 ①	65.8	32.3	1.9	X
Ru20 ②	50.7	37.6	11.7	X
Ru20 ③	51.1	35.1	13.8	X
Ru20 ④	51.3	27.4	21.3	X

The observed regions correspond to different numbers as indicated in Fig. 2. Regions exhibiting martensite twins are specially marked in the last row.

substantial impact on the stability of the B2 phase and the martensitic transformation process.

The shape memory effect was experimentally determined from the ST test on Ru0, Ru6.25, and Ru12.5 as depicted in Figures 4(a) through (c), respectively. Notably, Ru6.25 and Ru12.5 exhibit unusual behaviors. In the case of Ru6.25, under applied stresses lower than 100 MPa, the specimen demonstrates expansion during the transformation, contrary to the expected contraction under compressive stress. This unusual expansion is linked to the volume increase during the martensitic transformation, where the volume of the martensite phase (B33) surpasses that of the austenite phase (B2), resulting in expansion during the transformation, as shown in Figure 1(f). Additionally, the observed expansion in Ru6.25 decreases with increasing applied stress, eventually leading to contraction in the direction of stress. This transition occurs with dislocation formation during the martensite transformation. As depicted in Figure 4(d), the plastic strain that forms during the martensitic transformation escalates with an increase in applied stress. When this strain exceeds the transformation volume expansion, the behavior transitions from expansion to contraction, highlighting the complex interplay between stress-induced dislocation formation and volume change, which influences the material's overall deformation behavior, as shown in point A and B in Figures 4(d) and (e). Conversely, the specimen consistently contracts under all levels of applied stress during the reverse transformation, as the reverse transformation has contraction behavior, aligning with the stress direction and showing no expansion-to-contraction transition. Upon heating to temperatures exceeding 600 °C after the reverse transformation, an increase in dislocation introduction occurs, resulting in significant plastic strain, as indicated at point C in Figure 4(e). As depicted in Figure 4(b), Ru12.5 mirrors the behavior of Ru6.25, exhibiting a similar expansion-to-contraction transition during the martensitic transformation. However, the volume fraction of martensitic transformation in Ru12.5 is lower than that in Ru6.25, due to the persistence of the dendritic structure shown in Figure 2(c). This leads to smaller transformation strains and less plastic strain introduced during the martensitic transformation. Additionally, the notably lower transformation temperature of Ru12.5, compared to Ru6.25, results in fewer dislocations and reduced plastic strain following the reverse transformation. In contrast, the results for Ru0 are in line with standard thermal expansion patterns, exhibiting neither transformation strain nor recoverable strain, as shown in Figure 4(a). When exposed to temperatures above 600 °C, Ru0 also exhibits significant plastic deformation, similar to that observed in Ru6.25 and Ru12.5. Surprisingly, the deformation strain of Ru0 is lower compared to the Ru-added alloys, suggesting the need for further research to understand this discrepancy.

Despite these findings across the three alloys showing no transformation strain, the potential of the ZrPd series as shape memory alloys remains intact. The absence of a noticeable shape memory effect implies that the reorientation of martensite variants was not triggered under the conditions tested. Nonetheless, as demonstrated in Figure 4(f), the outcomes from a room temperature compression test on Ru0 reveal that the reorientation of martensite variants can be triggered at a stress level of 1500 MPa. Even though the required stress being significantly high, this finding suggests that by increasing the applied stress, it is indeed possible to initiate the variant reorientation.

Nevertheless, the noticeable plastic strain observed at temperatures exceeding 600 °C indicates that these alloys might not possess sufficient high-temperature strength. Even if variant reorientation is activated, the plastic strain developed at elevated temperatures will significantly reduce the recoverable strain, making the ZrPd series less suited for high-temperature shape memory alloy applications. This highlights the necessity for precise alloying and modification of the high-temperature properties. By adjusting the alloy composition to enhance high-temperature strength and adjusting the stress gap required to activate variant reorientation, there is a pathway to unlock the shape memory potential of the ZrPd series.

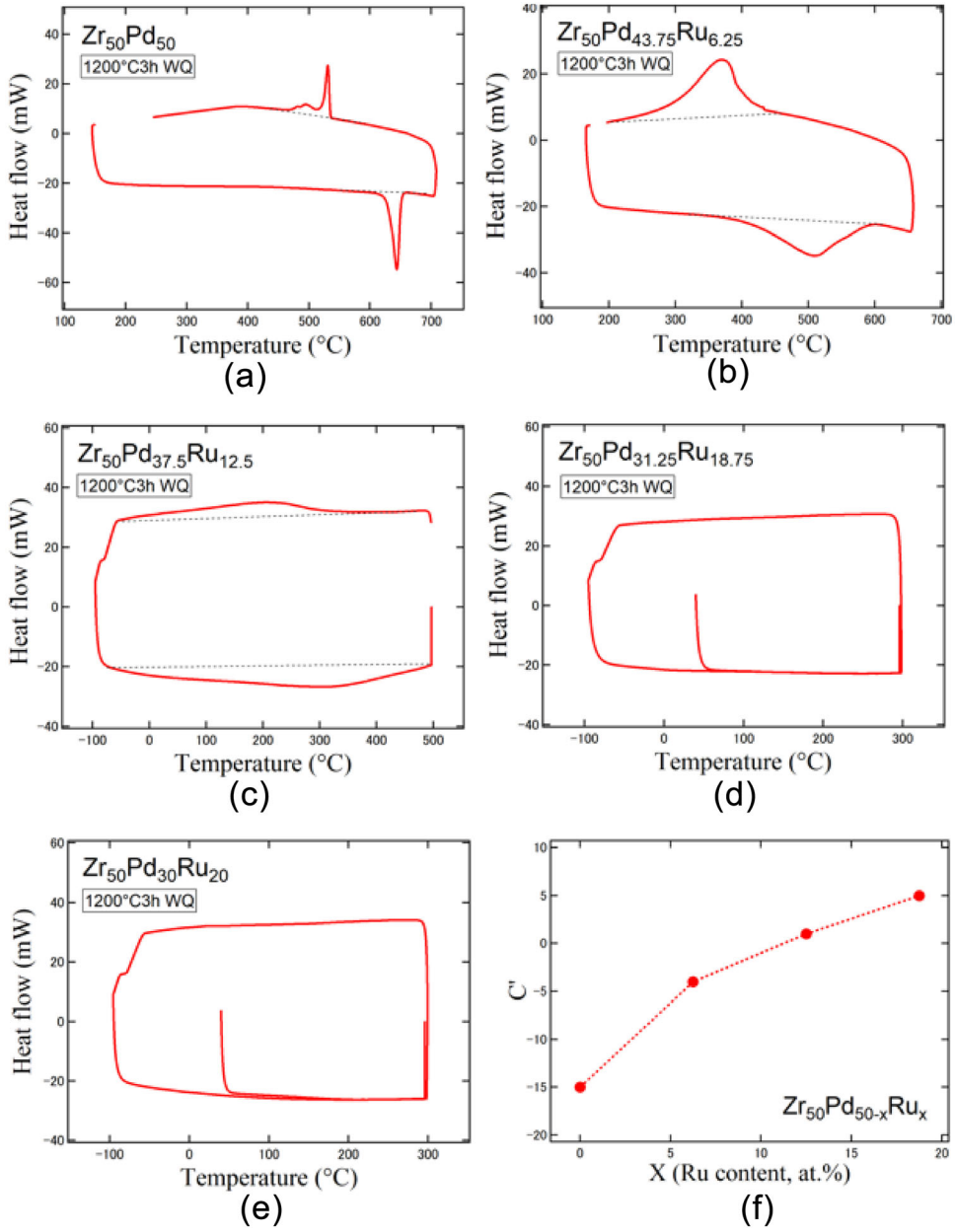

Fig. 3—DSC curves for (*a*) Ru0, (*b*) Ru6.25, (*c*) Ru12.5, (*d*) Ru18.75, (*e*) Ru20. (*f*) Value of elastic property C' with different Ru contents.

The experimental results have successfully validated Nkomo's theoretical predictions regarding the correlation between the C' parameter and martensitic transformation in ZrPdRu alloys. Through DSC analysis of Ru0, Ru6.25, and Ru12.5, along with the EDS results from the martensitic transformed region, it was observed that increasing in the Ru content and the C' parameter enhances the B2 phase's stability, significantly suppresses martensitic transformation, lowers the transformation temperature, and broadens the transformation temperature range. However, the expected shape memory effect was not observed in binary ZrPd alloys

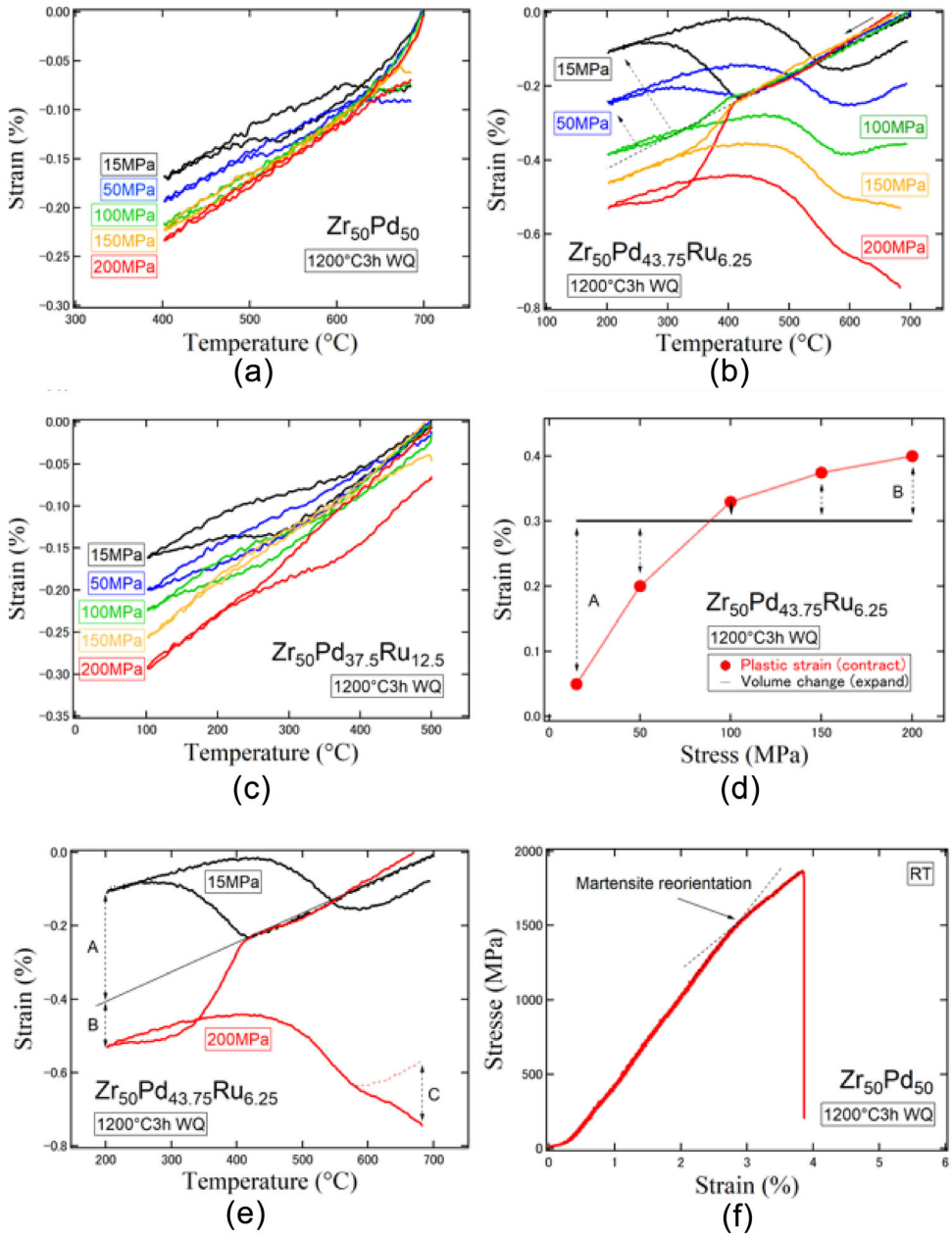

Fig. 4—Results of ST experiments for alloys (*a*) Ru0, (*b*) Ru6.25, (*c*) Ru12.5 under stress levels of 15, 50, 100, 150, and 200 MPa. (*d*) The transition in strain behavior of Ru6.25 under varying stress conditions. (*e*) Comparison of the strain behavior of Ru6.25 when subjected to 15 and 200 MPa stress levels. (*f*) The result of compression test of Ru0.

during strain–temperature testing, indicating an absence of martensite variant reorientation under applied stress. Despite this, the potential of ZrPd alloys as high-temperature shape memory materials remains promising. Through targeted alloying modifications, we can enhance the high-temperature shape memory behavior of these alloys, rendering them suitable for demanding applications in extreme conditions. This approach not only taps into their unique capabilities but also advances their potential in high-temperature shape memory technologies.

ACKNOWLEDGMENTS

This work was supported by Japan-NRF Joint Research Program, Grant number JPJSBP120226503. The authors appreciate that this study was partly supported by ''Precious Metals Research Grant of the TANAKA Memorial Foundation.''

FUNDING

Open Access funding provided by The University of Tokyo.

CONFLICT OF INTEREST

The authors declare that they have no conflict of interest.

REFERENCES

1. G.B. Kauffman and I. Mayo: *Chem. Educ.*, 1997, vol. 2, pp. 1–21.
2. Y. Yamabe-Mitarai: *Metals*, 2020, vol. 10, p. 1531.
3. L.A. Bendersky, J.K. Stalick, R. Portier, and R.M. Waterstrat: *J. Alloys Compd.*, 1996, vol. 236, pp. 19–25.
4. A. Al-hajry, M. Al-assiri, and N. Cowlam: *J. Phys. Chem. Solids*, 1998, vol. 59, pp. 1499–1505.
5. R.M. Waterstrat, A. Shapiro, and A. Jeremie: *J. Alloys Compd.*, 1999, vol. 290, pp. 63–70.
6. M. Matsuda, T. Nishimoto, Y. Morizono, S. Tsurekawa, and M. Nishida: *Intermetallics*, 2011, vol. 19, pp. 894–99.
7. M. Matsuda, K. Arai, M. Mitsuhara, Y. Yamabe-Mitarai, and M. Nishida: *J. Mater. Sci.*, 2021, vol. 56, pp. 5899–5909.
8. M. Matsuda, Y. Shinagawa, K. Takashima, M. Mitsuhara, and M. Nishida: *Mater. Trans.*, 2018, vol. 59, pp. 1567–73.
9. M. Matsuda, T. Nishiura, T. Yamamuro, and M. Nishida: *Metals*, 2018, vol. 8, p. 366.
10. D. Nkomo, B. Ngobe, M. Phasha, and Y. Yamabe-Mitarai: *Mater. Today: Proc.*, 2023. in press.
11. B.S. Ngobe, M.J. Phasha, and I.A. Mwamba: *Suid-Afrikaanse Tydskrif vir Natuurwetenskap en Tegnologie*, 2021, vol. 40, pp. 205–11.
12. B.S. Chen, J.L. Liu, C. Wang, X.Y. Guan, J.Q. Song, and Y.Z. Li: *J. Alloys Compd.*, 2016, vol. 662, pp. 484–88.
13. R.M. Waterstrat and R. Kuentzler: *J. Alloys Compd.*, 2003, vol. 359, pp. 133–38.